Check for updates

AGU ADVANCING EARTH AND SPACE SCIENCES

Geophysical Research Letters

RESEARCH LETTER
10.1029/2025GL118277

Overturning Circulation of the North Atlantic Subtropical Gyre Computed in Density Coordinates at 26°N

D. A. Smeed[1], W. E. Johns[2], R. H. Smith[3], T. Petit[1], E. L. McDonagh[1,4], D. Rayner[1], D. L. Volkov[3,5], S. Elipot[2], J. B. Kajtar[1], B. A. King[1], Y. L. Firing[1], and B. I. Moat[1]

[1]National Oceanography Centre, Southampton, UK, [2]Rosenstiel School of Marine, Atmospheric, and Earth Science, University of Miami, Coral Gables, FL, USA, [3]Atlantic Oceanographic and Meteorological Laboratory, NOAA, Miami, FL, USA, [4]NORCE, Norwegian Research Centre, Bjerknes Centre for Climate Research, Bergen, Norway, [5]Cooperative Institute for Marine and Atmospheric Studies, University of Miami, Miami, FL, USA

Key Points:

- A method for calculating overturning circulation in density coordinates from the data available at 26°N is presented
- Use of density coordinates highlights the shallow cell associated with overturning in the subtropical gyre
- The Atlantic Meridional Overturning Circulation calculated in density space is slightly greater than in depth space, but the time series are very similar

Supporting Information:

Supporting Information may be found in the online version of this article.

Correspondence to:

D. A. Smeed,
das@noc.ac.uk

Citation:

Smeed, D. A., Johns, W. E., Smith, R. H., Petit, T., McDonagh, E. L., Rayner, D., et al. (2026). Overturning circulation of the North Atlantic subtropical gyre computed in density coordinates at 26°N. *Geophysical Research Letters*, *53*, e2025GL118277. https://doi.org/10.1029/2025GL118277

Received 17 JUL 2025
Accepted 20 FEB 2026

Abstract The RAPID-MOCHA-WBTS array in the subtropical gyre of the North Atlantic has measured the Atlantic Meridional Overturning Circulation (AMOC) and the overturning streamfunction in depth coordinates since 2004. Here we show that the overturning streamfunction in density coordinates can be estimated by combining data from the RAPID-MOCHA-WBTS array with repeated shipboard measurements from the Florida Straits and Argo data. The streamfunction in density coordinates highlights the shallow overturning cell associated with the subtropical gyre circulation, a feature that is obscured in depth coordinates. The AMOC calculated in density space is slightly greater than in depth space, but the variability of the time series are very similar with differences occurring when the streamfunction maximum occasionally switches from the main overturning cell to the shallow cell.

Plain Language Summary The Atlantic Meridional Overturning Circulation (AMOC) is a large system of ocean currents in the Atlantic Ocean that transports warm water northward near the surface and returns colder, deeper water southward. As such, it plays an important role in global and regional variability. In this paper we compare two different calculations of the AMOC, one is determined from the distribution of ocean currents with depth in the ocean and the other analyses the distribution of ocean currents according to the density of sea water. The results of the two analyses are similar, but the use of density reveals aspects of the circulation within the subtropical ocean that are obscured when depth is used.

1. Introduction

In the early 2000s oceanographers sought to make the continuous measurements that are needed to quantify long-term changes in the Atlantic Meridional Overturning Circulation (AMOC) (Hirschi et al., 2003; Send et al., 2002). Variability of ocean circulation on eddy timescales is much larger than the variability on decadal timescales, and so occasional observations are not sufficient to detect decadal change, because the observations may be aliased by eddy variability. Johns et al. (2005) and Kanzow et al. (2006) showed that, by making use of geostrophic balance, meridional mass transport across ocean basins could be measured with only a few dynamic-height moorings. This insight demonstrated that continuous measurement of the AMOC was possible. The first basin-wide AMOC observing array, the RAPID-MOCHA-WBTS array, hereafter the RAPID array, was established in 2004. Direct measurements of velocity are made close to the ocean boundary, but a large part of the transport is measured using dynamic height moorings that are thousands of kilometers apart (Rayner & Kanzow, 2011), enabling measurement of the AMOC with relatively few resources. Following the success of the RAPID array other AMOC observing arrays have been implemented (Frajka-Williams et al., 2019), including the OSNAP array in the subpolar North Atlantic (Lozier et al., 2019).

The AMOC measured by the RAPID array is defined as the maximum of the overturning streamfunction evaluated by integrating meridional transport across the basin on pressure surfaces. In contrast the AMOC derived from the OSNAP array is defined using a streamfunction calculated by integrating meridional transport along lines of constant density. The streamfunction in density coordinates is generally regarded as being more closely aligned with the rates of water mass transformation (Zhang, 2010), and this is particularly important in the subpolar ocean where isopycnals slope more steeply than in the subtropical gyre. The downside of using the density coordinate streamfunction is that transport integrated along isopycnals cannot accurately be measured using endpoint measurements in the same way that transport on a pressure surface can be measured.

© 2026. The Author(s).
This is an open access article under the terms of the Creative Commons Attribution License, which permits use, distribution and reproduction in any medium, provided the original work is properly cited.

Consequently, the calculation of the AMOC in density coordinates is more complex and requires data at many more locations.

In contrast to the subpolar ocean, isopycnals in the subtropical ocean slope less steeply and it is generally expected that the AMOC calculated in density space is similar to that calculated in depth coordinates (Johnson et al., 2019). However, analysis of the streamfunction in density coordinates provides insight into water mass transformation (e.g., Xu et al., 2018) and Foukal and Chafik (2024) noted that the circulation associated with the formation of subtropical mode waters (STMW) is not apparent in the depth space streamfunction and made the case for calculating overturning in density space at all observing arrays. In this paper, we show how repeated shipboard measurements from the Florida Straits and the Argo array can be used, along with measurements from the RAPID array, to obtain the data required to calculate the overturning streamfunction in density space. The density-space streamfunction and the depth-based streamfunction are then compared and key differences between them are highlighted.

2. Data

2.1. The RAPID Array

The location of the RAPID array is shown in Figure 1a. There are several components to the array that are combined to calculate the depth-based overturning streamfunction: (a) transport through the Florida Straits is measured via the induced voltage in a subsea cable calibrated by shipboard measurements (Volkov et al., 2024); (b) transport on the steep slope east of the Bahamas is measured by an array of moored current meters, referred to as the western boundary wedge (WBW, Johns et al., 2008); and (c) east of the WBW, geostrophic transport is measured using dynamic height moorings located on the eastern and western boundaries.

To determine heat and freshwater transport, temperature and salinity values are required across the whole basin. For these, RAPID produces an objective analysis (OA) of Argo profiles (Johns et al., 2023; McDonagh et al., 2015). Further details are given in Supporting Information S1.

The RAPID data sets are updated following each mooring recovery. In this work, we use the data sets published by Moat et al. (2026), covering the period from April 2004 to February 2024.

2.2. Data From the Florida Straits, the Abaco Section, and the World Ocean Atlas

NOAA's Atlantic Oceanographic and Meteorological Laboratory conducts regular surveys of the Florida Straits at 27°N. There are nine oceanographic stations across the 90 km wide strait. Between 2000 and 2024, 108 surveys were completed, each including Conductivity-Temperature-Depth (CTD), Lowered Acoustic Current Profiler (LADCP), and Shipboard Acoustic Doppler Current Profiler (SADCP) measurements. These data are interpolated onto a regular grid, and tidal signals are removed from the velocity measurements. The resulting mean velocity and potential density fields are shown in Figure 1b. This repeat-section data set enables us to estimate the transport through the Florida Straits as a function of density much more accurately than was possible in 2004 when the RAPID array was first implemented.

East of the Bahamas, CTD data along the Abaco line at 26.5°N are collected roughly annually. The locations of the CTDs and the extent of the section varies between each of the 31 occupations of the line since 2000 (Chomiak et al., 2022).

Below the depth of Argo (1,800 m) and east of 74°W, we use temperature and salinity data from the World Ocean Atlas analysis for the period 1991–2020 (WOA2023, Reagan et al., 2024).

2.3. Data From the OSNAP Array

Using the time series of the overturning streamfunction as a function of σ_0 published by the OSNAP project (Fu et al., 2025), we have calculated the transport of water masses defined by potential density for comparison with the results from RAPID.

19448007, 2026, 5, Downloaded from https://agupubs.onlinelibrary.wiley.com/doi/10.1029/2025GL118277 by NICE, National Institute for Health and Care Excellence, Wiley Online Library on [11/03/2026]. See the Terms and Conditions (https://onlinelibrary.wiley.com/terms-and-conditions) on Wiley Online Library for rules of use; OA articles are governed by the applicable Creative Commons License

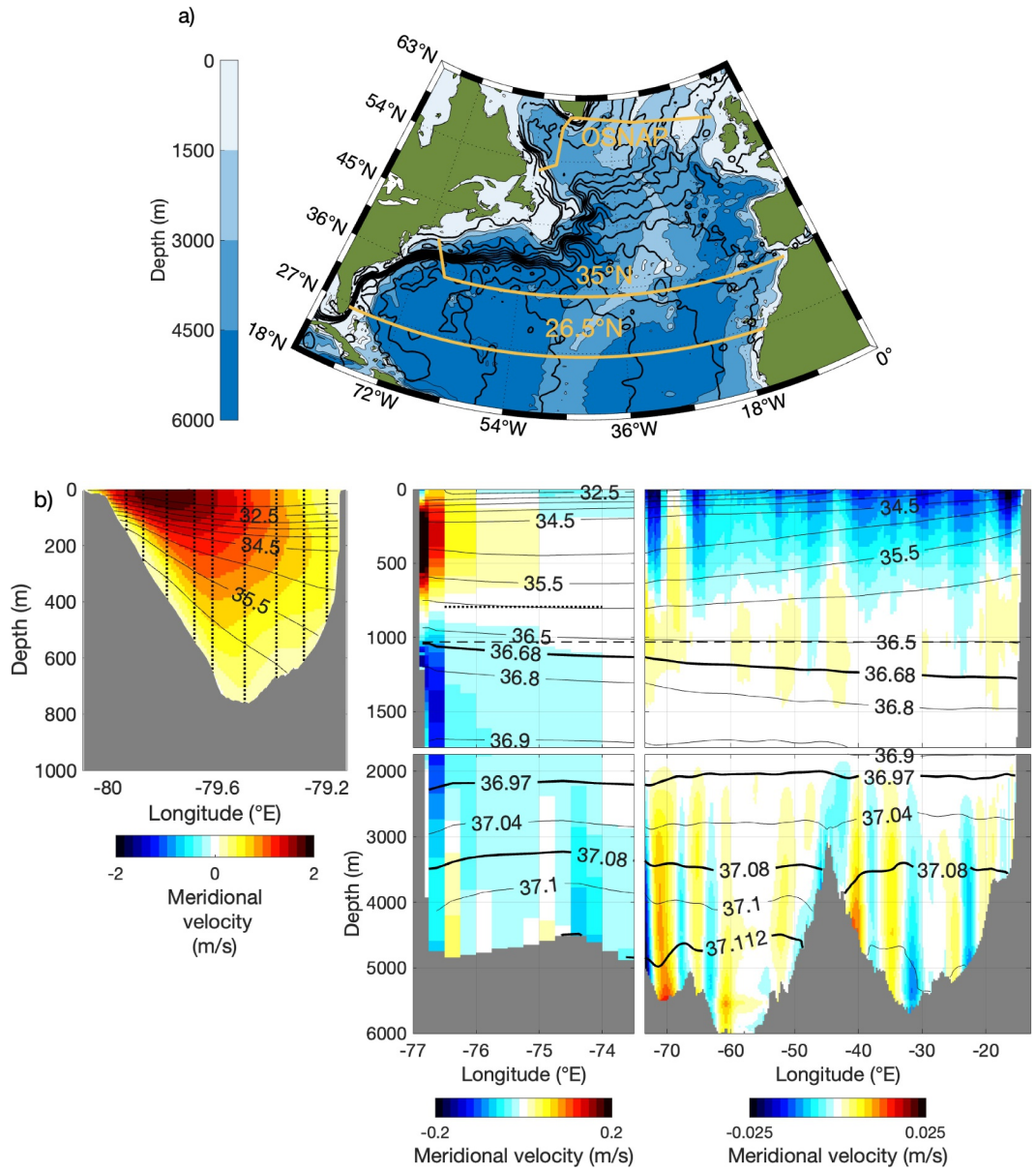

Figure 1. (a) The location the RAPID array, the OSNAP array and the 35°N section (Le Bras et al., 2023). Black lines are contours of sea surface height (contour interval 0.1 m, data from Copernicus). Contours of water depth at 1,000, 3,000, and 5,000 m are shown by shades of blue. (b) Mean meridional velocity and σ_2. Left: mean of shipboard sections acquired in the Florida Straits between 2004 and 2024. Vertical dotted lines show the locations of the 9 repeat stations. Middle and right: mean of estimated meridional velocity east of the Bahamas. Note the different color scale in each plot. Black lines show contours of σ_2; the same contours are used in each part. Bold contours highlight the values used to separate water masses whose transports are shown in Figure 2d. The horizontal dashed line illustrates the depth of maximum of the mean depth-space streamfunction. The break between the upper and lower parts of the middle and right-hand plots is at 1,740 m, the level of no motion east of 74°W. The dotted line at 795 m is the level of no motion east of the western boundary wedge and west of 74°W.

3. Estimation of the Streamfunction and AMOC

3.1. Calculation in Depth Space

Here we present a summary of the method described by McCarthy et al. (2015). The calculation of the overturning streamfunction in depth space is done in four parts: the Florida Straits transport (see Section 2.2 above), the WBW

19448007, 2026, 5, Downloaded from https://agupubs.onlinelibrary.wiley.com/doi/10.1029/2025GL118277 by NICE, National Institute for Health and Care Excellence, Wiley Online Library on [11/03/2026]. See the Terms and Conditions (https://onlinelibrary.wiley.com/terms-and-conditions) on Wiley Online Library for rules of use; OA articles are governed by the applicable Creative Commons License

19448007, 2026, 5, Downloaded from https://agupubs.onlinelibrary.wiley.com/doi/10.1029/2025GL118277 by NICE, National Institute for Health and Care Excellence, Wiley Online Library on [11/03/2026]. See the Terms and Conditions (https://onlinelibrary.wiley.com/terms-and-conditions) on Wiley Online Library for rules of use; OA articles are governed by the applicable Creative Commons License

transport (see Section 2.1 above), the Ekman transport, and the transport east of the WBW. We refer to the latter as the "interior transport."

The meridional Ekman transport is derived from the ERA5 reanalysis estimates of zonal wind stress (Hersbach et al., 2023) and is assumed to be distributed uniformly over the upper 100 m.

The geostrophic transport east of the WBW is calculated from dynamic height moorings. Data from moorings are concatenated vertically (McCarthy et al., 2015), to derive eastern and western dynamic height profiles with a reference level of 4,820 db. The difference between these, plus an additional term due to the mean dynamic height difference across the mid-Atlantic Ridge, gives a geostrophic transport profile. Below 4,820 db, a time-invariant profile of transport shear is defined that represents the gradient of transport within Antarctic Bottom Water (AABW).

The transport at the reference level (4,820 db) is determined by requiring that, when all four transport components are summed, there is no net meridional transport. A uniform velocity is added throughout the interior region so that this condition is met. Note that, as the additional velocity is uniform, it has no vertical shear and geostrophic balance is not altered, but, because the width of the interior region varies with depth, there is a vertical gradient of transport. We refer to the profile of transport that arises from the reference level velocity as the "compensation transport." The compensation transport is added to the geostrophic transport to obtain the total transport in the interior.

3.2. Calculation in Density Space

As noted in the introduction, calculation of a streamfunction in density coordinates requires estimates of meridional velocity and density throughout the section. Temperature and salinity across the ocean interior are obtained from the OA and then velocity is calculated using geostrophy (similar to the methodology of Johns et al. (2023)). Profiles of accumulated transport as a function of density are then calculated separately for each of the three regions: the ocean interior, the WBW, and the Florida Straits. The boundary between the WBW and ocean interior is at the location of the mooring WB3, situated close to the 4,800 m isobath about 50 km east of Abaco Island. Summing these profiles gives the overturning streamfunction in density space. In this work we use potential density relative to 2,000 db, and the calculation is made at 10-day resolution. The potential density anomaly (σ_2) levels have variable spacing from 0.1 kg m^{-3} at $\sigma_2 = 30.0$ to 0.001 kg m^{-3} at $\sigma_2 = 37.15$ kg m^{-3}.

3.2.1. Interior Ocean

In the interior ocean, we estimate variables on a longitude grid with resolution 0.25° from 76.75°W to 14°W, and on a pressure grid of 20 db resolution from the surface to 6,120 db. Above 1,800 db, temperature and salinity are obtained from the Argo OA. Below 1,800 db and west of 74°W, data are derived from the WBTS CTD sections. Optimal interpolation of WBTS data in time is made using a Gaussian weight function with a time scale of 1 year. Below 1,800 db and east of 74°W, we use WOA2023 data that are constant in time. Dynamic height is calculated at each longitude with a reference level of 800 db west of 74°W, consistent with previous studies on the Antilles Current by Johns et al. (2008) and Meinen et al. (2019) and with analysis of the deep western boundary current transport by Biló and Johns (2020). East of 74°W, the reference level is 1,760 db, or the bottom when the water depth is shallower, this corresponds with the depth above which Argo data is available. The dynamic height profiles are then differenced to derive geostrophic transport in each 0.25° of longitude. Finally, a small adjustment in velocity, uniform with longitude, is added at each depth so that the profile of longitudinally integrated transport matches that calculated by the endpoint methodology used when estimating the streamfunction in depth space. Typically, the adjustment velocity is of the order of 0.001 ms^{-1}, further details are given in Supporting Information S1, where the sensitivity of the results to the choice of reference level is also examined.

The Ekman transport is derived from surface stress at each longitude and is assumed to be distributed uniformly over the upper 100 m.

The profile of meridional transport as a function of pressure at each longitude is integrated down from the surface to obtain a profile of accumulated transport which is then interpolated onto the density grid using the profile of density for that time and location. Finally, the profiles of accumulated transport as a function of density are summed across all longitudes to obtain a single profile of accumulated transport for the whole interior region.

19448007, 2026, 5, Downloaded from https://agupubs.onlinelibrary.wiley.com/doi/10.1029/2025GL118277 by NICE, National Institute for Health and Care Excellence, Wiley Online Library on [11/03/2026]. See the Terms and Conditions (https://onlinelibrary.wiley.com/terms-and-conditions) on Wiley Online Library for rules of use; OA articles are governed by the applicable Creative Commons License

3.2.2. The Florida Straits

For each of the 108 shipboard sections we follow a similar procedure to that used in the interior ocean, except that the velocities here are directly measured by SADCP/LADCP rather than being geostrophic estimates. At each longitude, velocity is integrated down from the surface to obtain a profile of accumulated transport, then the density profile is used to interpolate the accumulated transport onto the density grid, and then the profiles from each longitude are summed to obtain a single profile of accumulated transport as a function of density at the time for each section. Next, we separate the accumulated transport profiles for each section into three components:

1. A mean seasonal cycle determined by a least squares fit to the data of a function with two harmonics (annual and semi-annual).
2. A slowly varying interannual component. After removing the seasonal cycle, we use an optimal interpolation in time using a Gaussian weight function with a time scale of 1 year.
3. A residual. The residual, after fitting of the two above components, at each level is regressed against the total transport anomaly at the time of each section (see Figure S3 in Supporting Information S1). The uncertainty associated with the regression is small and is shown in Figure S4 in Supporting Information S1.

To calculate a profile of transport every 10-days we sum the mean seasonal cycle (1, above), the slowly varying interannual component (2, above), and a third term computed by multiplying the regression coefficients, derived in (3) above, by a transport anomaly that is the cable-based estimate of total transport minus the sum of the mean annual cycle and interannual component of the total transport.

3.2.3. Western Boundary Wedge

The profiles of transport in the WBW are the same as those used when estimating the streamfunction in depth space. Profiles of temperature and salinity are also obtained from moorings WB2 and WB3. Interpolation is then used to derive profiles of accumulated transport as a function of density.

4. The Overturning Streamfunctions in Depth and Density Space

The mean streamfunction in depth space, $\overline{\Psi_z}$, and its counterpart calculated in density space, $\overline{\Psi_\sigma}$, are shown in Figure 2. The total range of density in the subtropics varies seasonally but is about 6 kg m^{-3}. However, the total change in σ_2 below 1,000 db is less than 0.5 kg m^{-3}, thus the streamfunction in σ_2 space naturally emphasizes details in the thermocline (Figure S5a in Supporting Information S1). In Figures 2 and 3 a log scale is used so that details of the transport below the thermocline can be seen more easily.

When we separate the streamfunction into the accumulated transport flowing through the Florida Straits and that east of the Bahamas (Figures 3b and 3c, Figure S5 in Supporting Information S1), we see that there is at least 10 Sv flowing north through the Florida Straits for$\sigma_2 < 34$ kg m^{-3}, but there is less than 1 Sv of net southward flow of these waters east of the Bahamas. The profile of $\overline{\Psi_\sigma}$ is almost constant between $\sigma_2 = 34$ kg m^{-3} and $\sigma_2 = 35.5$ kg m^{-3} with a small secondary maximum at about $\sigma_2 = 34.6$ kg m^{-3} below which there is a small (<0.5 Sv) net southward transport. The streamfunction then increases to a maximum at $\sigma_2 = 36.68$ kg m^{-3}.

The maximum of the meridional overturning streamfunction is usually used to quantify the AMOC, and we define AMOC$_z$ and AMOC$_\sigma$ to be the maxima of the depth-space streamfunction and density-space streamfunction, respectively. There is a clear correspondence between the maxima of the two mean profiles, 16.9 Sv at 1,030 m for AMOC$_z$ and 17.4 Sv at $\sigma_2 = 36.68$ kg m^{-3} for AMOC$_\sigma$. The $\sigma_2 = 36.68$ kg m^{-3} isopycnal slopes upward as it approaches the western boundary (Figure 1), where it is close to 1,030 m, but across most of the basin the isopycnal surface lies below 1,030 m. Thus, in density coordinates, more northward flowing intermediate water is included in the upper limb of the AMOC and less is in the lower limb resulting in 0.4 Sv more overturning.

The time series of AMOC$_z$ and AMOC$_\sigma$ (Figure 2c) are very similar. The AMOC evaluated in density coordinates is on average 0.5 Sv stronger than that calculated in depth space. However, there are times when the difference is much greater. This mostly occurs when AMOC$_z$ is weak and when the density of maximum overturning switches from the deep cell to the shallow cell. Here "deep cell" refers to the main overturning cell that extends throughout the North Atlantic and "shallow cell" refers to the near surface cell that is found within the subtropical gyre.

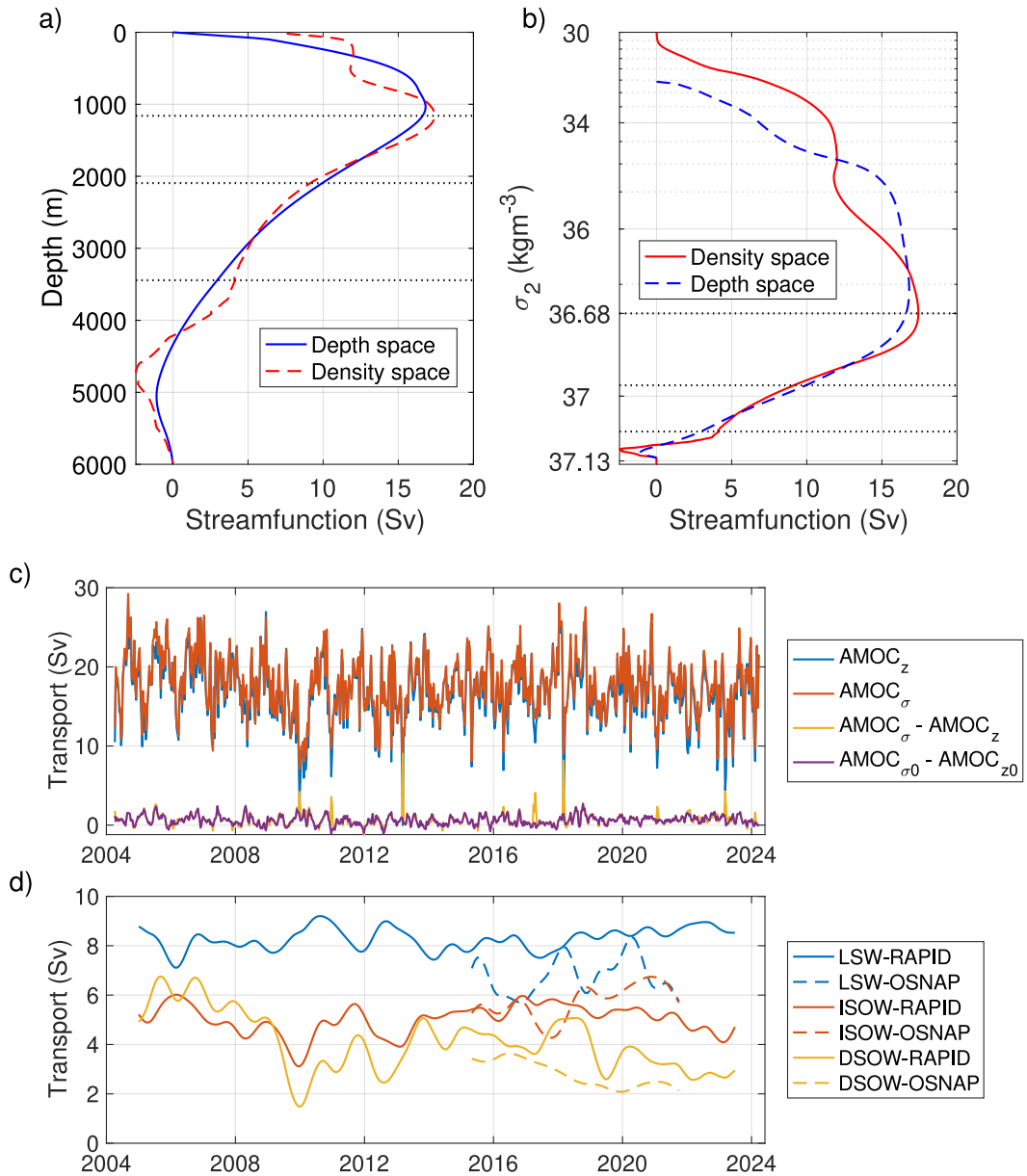

Figure 2. Comparison of the overturning streamfunctions evaluated in depth space and density space. (a) Mean streamfunction, $\overline{\Psi_z}$, calculated in depth space, and (b) $\overline{\Psi_\sigma}$ calculated in density space. The relationship between depth and density varies in space and time so $\overline{\Psi_z}$ cannot be exactly described as a function of density, and $\overline{\Psi_\sigma}$ cannot be described as a function of depth, however, to aid comparison of the two streamfunctions we have plotted $\overline{\Psi_\sigma}$ on (a) using depth determined from a mean profile of density in the western basin. Similarly, $\overline{\Psi_z}$, is shown in panel (b). (c) Time series of AMOC$_z$ and AMOC$_\sigma$. Also shown are the differences AMOC$_\sigma$ − AMOC$_z$ and AMOC$_{\sigma 0}$ − AMOC$_{z0}$, where AMOC$_{z0}$ is the streamfunction evaluated at the fixed depth of 1,030 m, and AMOC$_{\sigma 0}$ is evaluated at the $\sigma_2 = 36.68$ kg m^{-3}. (d) Transports of water masses determined by density from RAPID (continuous lines) and OSNAP (dashed lines). An 18-month filter has been applied. The values of σ_2 that define the water masses are illustrated by horizontal dotted lines in panel (b) and the corresponding depths (derived from the mean density profile in the western basin) are shown in panel (a).

In Figure 2d we show the transports of water masses defined by the values of σ_2. Labrador Sea Water (LSW) is defined by $36.68 < \sigma_2 < 36.97$ kg m^{-3}, Iceland-Scotland Overflow Water (ISOW) has $36.97 < \sigma_2 < 37.08$ kg m^{-3}, and Denmark Straits Overflow Water (DSOW) is defined by $\sigma_2 > 37.08$ kg m^{-3} (van Sebille et al., 2011). For comparison we also show the corresponding transports for the OSNAP array where the upper bounds of LSW, ISOW, and DSOW are the σ_0 isopycnals 27.61, 27.80, and 27.89 kg m^{-3}. Mean values and trends are shown in

19448007, 2026, 5, Downloaded from https://agupubs.onlinelibrary.wiley.com/doi/10.1029/2025GL118277 by NICE, National Institute for Health and Care Excellence, Wiley Online Library on [11/03/2026]. See the Terms and Conditions (https://onlinelibrary.wiley.com/terms-and-conditions) on Wiley Online Library for rules of use; OA articles are governed by the applicable Creative Commons License

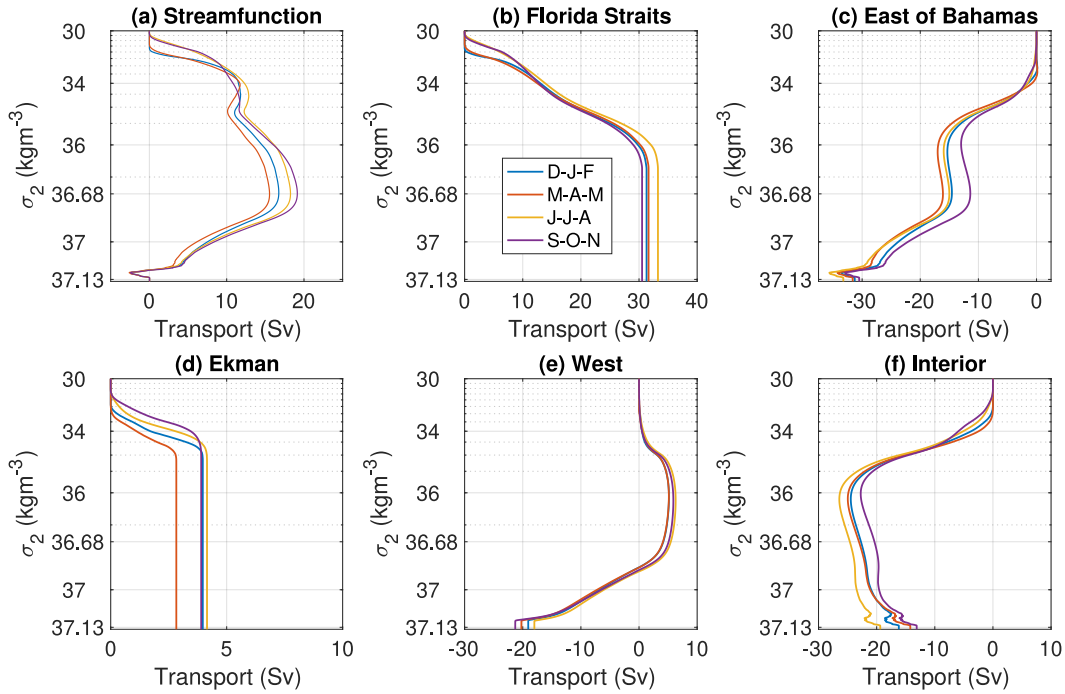

Figure 3. Seasonal cycle of the overturning streamfunction and its component parts. (a) Ψ_σ calculated in density space. (b) The accumulated transport through the Florida Strait and (c) the accumulated total transport east of the Bahamas. The flow east of the Bahamas is separated further into: (d) the Ekman transport, (e) flow adjacent to the western boundary (west of 74°W) and (f) the remaining flow east of 74°W. Mean profiles are shown for each of the four seasons. In each case transport is accumulated with increasing density starting from $\sigma_2 = 30$ kg m^{-3}. Note that the range of transport is the same in panels (b, c, e, and f), but different ranges are used in panels (a, d).

Tables S2 and S3 in Supporting Information S1. Note that we have not separated DSOW from AABW. All AABW that flows north from 26°N is upwelled and returns south and we believe that the net transport below $\sigma_2 = 37.08$ kg m^{-3} is a more useful variable when comparing with the OSNAP data.

There is a long-term declining trend in the transport of DSOW at RAPID, however, there are no trends in LSW or ISOW transport. The mean density space streamfunction profile indicates that there is a minimum in transport between DSOW and ISOW (c. 3,500 m depth), and it seems that more of the former transport occurs further from the continental slope (Figure 1b, see also Biló and Johns (2020)). Changes in the transport of LSW are often anti-correlated with changes in the transport of ISOW suggesting that there is no clear separation between these water masses. Often a single classification of Upper North Atlantic Deep Water is used, instead of separate LSW and ISOW water masses, when analyzing transports in the subtropical gyre (e.g., Moat et al., 2020).

The minimum of $\overline{\Psi_\sigma}$ suggests that there is about 2.5 Sv northward transport of AABW, compared with 1 Sv in depth coordinates. This difference is consistent with the analysis of Frajka-Williams et al. (2011). However, there are no measurements of geostrophic shear below 4,820 db. There is thus significant uncertainty about the variability in the transport of AABW (see Supporting Information S1 for further discussion).

Kanzow et al. (2010) showed that there is a significant annual cycle of AMOC$_z$ at 26.5°N. At the level of the mean streamfunction maximum, the annual cycle of overturning in density space is very similar to that evaluated depth space (Figure S6 in Supporting Information S1), both have an annual range of about 5 Sv to which the interior ocean makes the largest contribution. However, Figure 3a shows that the shape of the overturning streamfunction Ψ_σ changes through the seasons. In particular, a more pronounced secondary maximum is seen in spring at $\sigma_2 \approx 34$ kg m^{-3} when there is roughly 1.5 Sv of southward flow between $\sigma_2 = 34$ kg m^{-3} and $\sigma_2 = 35.2$ kg m^{-3}; this is largely due to the increase of density in the seasonal thermocline which results in more of the southward gyre recirculation occurring for $\sigma_2 > 34$ kg m^{-3} and less occurring for lighter densities (Figure 3f). Weaker northward flow of the Florida Straits (Figure 3b) and Antilles Current (Figure 3e) in the spring also contribute to a seasonal change in the shape of the overturning streamfunction.

19448007, 2026, 5, Downloaded from https://agupubs.onlinelibrary.wiley.com/doi/10.1029/2025GL118277 by NICE, National Institute for Health and Care Excellence, Wiley Online Library on [11/03/2026]. See the Terms and Conditions (https://onlinelibrary.wiley.com/terms-and-conditions) on Wiley Online Library for rules of use; OA articles are governed by the applicable Creative Commons License

5. Discussion

In a modeling study, Tooth et al. (2024) presented the time-mean density space streamfunction at 26°N (their Figure 3f). The streamfunction of Tooth et al. (2024) has two maxima. The global maximum is at $\sigma_0 \sim 27.5$ kg m^{-3} and there is a secondary maximum at $\sigma_0 \sim 25$ kg m^{-3}. Based on a Lagrangian analysis, Tooth et al. (2024) interpreted the streamfunction as a superposition of a shallow overturning cell and a deep cell, with the shallow cell being a representation of the subtropical gyre circulation in which water parcels are transformed to greater densities as they spiral down within the gyre (Berglund et al., 2022). Our Eulerian data does not allow us to separate the two cells, but our results are broadly consistent with this interpretation. However, the minimum between the two maxima of our mean streamfunction is less pronounced than that in the model This suggests that the maximum of the shallow cell occurs at a slightly greater value of σ_2 than in the model, and that the southward recirculation of the shallow cell and the northward flow of the deep cell almost balance for $\sigma_2 > 34$ kg m^{-3} and $\sigma_2 < 35.5$ kg m^{-3}. The difference in the shape of the streamfunction between model and observations appears to be due to too much gyre recirculation in the upper 100 m in the model (Tooth et al., 2024), and the AMOC being about 2 Sv weaker in the model. Note too that the secondary maximum is most evident in our observational analysis in spring when the AMOC is at its weakest in the annual cycle.

Le Bras et al. (2023) made estimates of overturning in density space based on Line-W moorings, along with float and altimeter data nominally at 35°N (Figure 1), close to the inter-gyre region. The range of densities at this latitude is less than at 26°N, and the slope of isopycnal surfaces is greater. Like our results, the density coordinate AMOC is larger than the depth space version but the difference, on average 2.3 Sv, is larger than that at 26°N, as might be expected given the more strongly sloping isopycnals. In density space the mean streamfunction calculated by Le Bras et al. (2023) has a secondary maximum of about 8 Sv at $\sigma_2 = 35$ kg m^{-3}, and Le Bras et al. (2023) identified this with the formation of subtropical mode waters (STMW). Some of the STMW transformation occurs upstream of Line-W, so it could be expected that the streamfunction associated with the subtropical gyre cell is less than the streamfunction value for $\sigma_2 = 35$ kg m^{-3} at 26°N (12 Sv).

Moat et al. (2020) noted that the reduction in AMOC$_z$ since 2004 is apparent in the transport of lower North Atlantic Deep Water (defined as being between 3,000 and 5,000 m) but there has been very little change in the transport of upper North Atlantic Deep Water (1,100–3,000 m). A similar picture is seen when evaluating transport in density classes (Figure 2d). The long-term trend in the transport of DSOW is similar to the trend in the AMOC (Table S2 in Supporting Information S1). There is a similar decreasing trend of DSOW transport at OSNAP, but, in contrast to our observations at 26°N, there is not a corresponding decrease in the AMOC. Koman et al. (2024) attributed the reduction in the deep western boundary current east of Greenland to the changing properties of deep water which resulted in a reduced volume below a fixed isopycnal. Considering the whole OSNAP section (Figure 2d and Table S2 in Supporting Information S1) we see that the reduction in DSOW transport is balanced by an increase of the transport of ISOW suggesting that the changing properties of deep waters is also the reason for the apparent trend in DSOW at OSNAP. Note too that the trends in the RAPID data evaluated over 2014–2022 period, when we have OSNAP data, are significantly different from those evaluated using the full 20 years of RAPID observations (Table S3 in Supporting Information S1) and these trends are not necessarily representative of longer-term changes.

6. Conclusions

The calculation of the streamfunction in density space requires significantly more data than does the depth space version. In particular, we have made use of the high-quality shipboard sections across the Florida Straits and data from the Argo array in the ocean interior. Very little data were available from these when the RAPID program started in 2004. These data are also necessary for accurate estimation of heat and freshwater transport. To continue monitoring the AMOC in the subtropical gyre it is essential to continue regular shipboard measurements in the Florida Straits and the deployment of Argo floats as well as measurements at 26°N.

Evaluating the streamfunction in density space highlights features of the circulation that are obscured in depth space, in particular, the overturning associated with the subtropical gyre recirculation. The shallow gyre cell is most evident in spring when the annual cycle of the deep overturning cell is at its weakest. The difference between AMOC$_\sigma$ and AMOC$_z$ is less at 26°N than at higher latitudes where isopycnals slope more; and the magnitude of the AMOC at 26°N is, on average, about 0.4 Sv stronger in density coordinates than in depth coordinates. This difference arises because the upper limb of the AMOC in density space includes more northward flowing

19448007, 2026, 5, Downloaded from https://agupubs.onlinelibrary.wiley.com/doi/10.1029/2025GL118277 by NICE, National Institute for Health and Care Excellence, Wiley Online Library on [11/03/2026]. See the Terms and Conditions (https://onlinelibrary.wiley.com/terms-and-conditions) on Wiley Online Library for rules of use; OA articles are governed by the applicable Creative Commons License

19448007, 2026, 5, Downloaded from https://agupubs.onlinelibrary.wiley.com/doi/10.1029/2025GL118277 by NICE, National Institute for Health and Care Excellence, Wiley Online Library on [11/03/2026]. See the Terms and Conditions (https://onlinelibrary.wiley.com/terms-and-conditions) on Wiley Online Library for rules of use; OA articles are governed by the applicable Creative Commons License

intermediate water transport than does the upper limb of the AMOC in depth space. Larger differences between $AMOC_\sigma$ and $AMOC_z$ occur when the streamfunction maximum occasionally switches from the deep to the shallow cell.

Conflict of Interest

The authors declare no conflicts of interest relevant to this study.

Data Availability Statement

The data sets used in this study are: the RAPID array freely available from http://www.rapid.ac.uk (Moat et al., 2026), the Western Boundary Time Series (https://www.aoml.noaa.gov/western-boundary-time-series), ERA5 reanalysis (https://cds.climate.copernicus.eu/datasets/reanalysis-era5-single-levels, Hersbach et al., 2023), World Ocean Atlas (https://www.ncei.noaa.gov/products/world-ocean-atlas, Reagan et al., 2024), the OSNAP project (https://www.o-snap.org/data-access/, Fu et al., 2025), the E.U. Copernicus Marine Service (https://doi.org/10.48670/moi-00148), and Argo (https://www.ocean-ops.org, Argo, 2000). Argo data were collected and made freely available by the International Argo Program and the national programs that contribute to it.

The results of the study (streamfunction in density space, along with the estimates of velocity, temperature and salinity at 26.5°N) have been published by Moat et al. (2026) with doi: 10.5285/48d0bf43-0598-ceb2-e063-7086abc062f1 and are freely available from https://rapid.ac.uk/data/data-download.

Version 1.0 of the Matlab code used to calculate the overturning streamfunction and plot the figures is preserved at https://doi.org/10.5281/zenodo.18432154 and is available under Apache License 2.0 (Smeed, 2026).

Acknowledgments

NOC authors are supported by Natural Environment Research Council Grants RAPID Evolution (NE/Y003551/1), ROCCA (NE/Y005287/1), and ATLANTiS (NE/Y005589/1). WJ and SE are supported by the US National Science Foundation under Grants 2148723 and 2334091. DLV and RHS are supported by the NOAA's Global Ocean Monitoring and Observing program (Grant 100007298) and by the NOAA Atlantic Oceanographic and Meteorological Laboratory. DLV was also supported by the Cooperative Institute for Marine and Atmospheric Studies (CIMAS), a cooperative institute of the University of Miami and NOAA, cooperative Agreement NA20OAR4320472. ELM is also supported by OceanICU funded by the European Union under Grant 101083922 and UK Research and Innovation (UKRI) under the UK government's Horizon Europe funding guarantee (Grants 10054454, 1006367, 10064020, 10059241, 10079684, 10059012, and 10048179). Views and opinions expressed are however those of the authors only and do not necessarily reflect those of the European Union or European Research Executive Agency. Neither the European Union nor the granting authority can be held responsible for them. We are very grateful for the comments and suggestions from the reviewers.

References

Argo. (2000). Argo float data and metadata from global data assembly centre [Dataset]. *(Argo GDAC). SEANOE*. https://doi.org/10.17882/42182

Berglund, S., Döös, K., Groeskamp, S., & McDougall, T. J. (2022). The downward spiralling nature of the North Atlantic subtropical gyre. *Nature Communications*, *13*(1), 2000. https://doi.org/10.1038/s41467-022-29607-8

Biló, T. C., & Johns, W. E. (2020). The deep Western boundary current and adjacent interior circulation at 24°–30°N: Mean structure and mesoscale variability. *Journal of Physical Oceanography*, *50*(9), 2735–2758. https://doi.org/10.1175/jpo-d-20-0094.1

Chomiak, L. N., Yashayaev, I., Volkov, D. L., Schmid, C., & Hooper, J. A. (2022). Inferring advective timescales and overturning pathways of the deep western boundary current in the North Atlantic through Labrador Sea water advection. *Journal of Geophysical Research: Oceans*, *127*(12), e2022JC018892. https://doi.org/10.1029/2022jc018892

Foukal, N., & Chafik, L. (2024). Consensus around a common definition of Atlantic overturning will promote progress. *Oceanography*, *37*(3), 11–15. https://doi.org/10.5670/oceanog.2024.507

Frajka-Williams, E., Ansorge, I. J., Baehr, J., Bryden, H. L., Chidichimo, M. P., Cunningham, S. A., et al. (2019). Atlantic meridional overturning circulation: Observed transport and variability. *Frontiers in Marine Science*, *6*, 260. https://doi.org/10.3389/fmars.2019.00260

Frajka-Williams, E., Cunningham, S. A., Bryden, H., & King, B. A. (2011). Variability of Antarctic bottom water at 24.5°N in the Atlantic. *Journal of Geophysical Research*, *116*(C11), C11026. https://doi.org/10.1029/2011jc007168

Fu, Y., Lozier, M. S., Bower, A. S., Burmeister, K., Biló, T. C., Cyr, F., et al. (2025). Meridional overturning circulation observed by the overturning in the subpolar North Atlantic program (OSNAP) array from August 2014 to July 2022 [Dataset]. *Georgia Tech Digital Repository*. https://doi.org/10.35090/gatech/78023

Hersbach, H., Bell, B., Berrisford, P., Biavati, G., Horányi, A., Muñoz Sabater, J., et al. (2023). ERA5 hourly data on single levels from 1940 to present [Dataset]. *Copernicus Climate Change Service (C3S) Climate Data Store (CDS)*. https://doi.org/10.24381/cds.adbb2d47

Hirschi, J., Baehr, J., Marotzke, J., Stark, J., Cunningham, S., & Beismann, J.-O. (2003). A monitoring design for the Atlantic meridional overturning circulation. *Geophysical Research Letters*, *30*(7), 1413. https://doi.org/10.1029/2002gl016776

Johns, W. E., Beal, L. M., Baringer, M. O., Molina, J. R., Cunningham, S. A., Kanzow, T., & Rayner, D. (2008). Variability of shallow and deep western boundary currents off The Bahamas during 2004–05: Results from the 26°N RAPID–MOC array. *Journal of Physical Oceanography*, *38*(3), 605–623. https://doi.org/10.1175/2007jpo3791.1

Johns, W. E., Elipot, S., Smeed, D. A., Moat, B., King, B., Volkov, D. L., & Smith, R. H. (2023). Towards two decades of Atlantic Ocean mass and heat transports at 26.5N. *Philosophical Transactions of the Royal Society A*, *381*(2262), 20220188. https://doi.org/10.1098/rsta.2022.0188

Johns, W. E., Kanzow, T., & Zantopp, R. (2005). Estimating ocean transports with dynamic height moorings: An application in the Atlantic deep western boundary current at 26°N. *Deep-Sea Research Part I*, *52*(8), 1542–1567. https://doi.org/10.1016/j.dsr.2005.02.002

Johnson, H. L., Cessi, P., Marshall, D. P., Schloesser, F., & Spall, M. A. (2019). Recent contributions of theory to our understanding of the Atlantic meridional overturning circulation. *Journal of Geophysical Research: Oceans*, *124*(8), 5376–5399. https://doi.org/10.1029/2019jc015330

Kanzow, T., Cunningham, S. A., Johns, W. E., Hirschi, J. J.-M., Marotzke, J., Baringer, M. O., et al. (2010). Seasonal variability of the Atlantic meridional overturning circulation at 26.5°N. *Journal of Climate*, *23*(21), 5678–5698. https://doi.org/10.1175/2010jcli3389.1

Kanzow, T., Send, U., Zenk, W., Chave, A. D., & Rhein, M. (2006). Monitoring the integrated deep meridional flow in the tropical North Atlantic: Long-term performance of a geostrophic array. *Deep-Sea Research Part I*, *53*(3), 528–546. https://doi.org/10.1016/j.dsr.2005.12.007

Koman, G., Bower, A. S., Holliday, N. P., Furey, H. H., Fu, Y., & Biló, T. C. (2024). Observed decrease in deep Western boundary current transport in subpolar North Atlantic. *Nature Geoscience*, *17*(11), 1–6. https://doi.org/10.1038/s41561-024-01555-6

Le Bras, I. A., Willis, J., & Fenty, I. (2023). The Atlantic meridional overturning circulation at 35°N from deep moorings, floats, and satellite altimeter. *Geophysical Research Letters*, *50*(10), e2022GL101931. https://doi.org/10.1029/2022gl101931

Lozier, M. S., Li, F., Bacon, S., Bahr, F., Bower, A. S., Cunningham, S. A., et al. (2019). A sea change in our view of overturning in the subpolar North Atlantic. *Science*, *363*(6426), 516–521. https://doi.org/10.1126/science.aau6592

McCarthy, G. D., Smeed, D. A., Johns, W. E., Frajka-Williams, E., Moat, B. I., Rayner, D., et al. (2015). Measuring the Atlantic meridional overturning circulation at 26°N. *Progress in Oceanography*, *130*, 91–111. https://doi.org/10.1016/j.pocean.2014.10.006

McDonagh, E. L., King, B. A., Bryden, H. L., Courtois, P., Szuts, Z., Baringer, M., et al. (2015). Continuous estimate of Atlantic Oceanic freshwater flux at 26.5°N. *Journal of Climate*, *28*(22), 8888–8906. https://doi.org/10.1175/jcli-d-14-00519.1

Meinen, C. S., Johns, W. E., Moat, B. I., Smith, R. H., Johns, E. M., Rayner, D., et al. (2019). Structure and variability of the Antilles current at 26.5°N. *Journal of Geophysical Research: Oceans*, *124*(6), 3700–3723. https://doi.org/10.1029/2018jc014836

Moat, B. I., Smeed, D. A., Frajka-Williams, E., Desbruyères, D. G., Beaulieu, C., Johns, W. E., et al. (2020). Pending recovery in the strength of the meridional overturning circulation at 26°N. *Ocean Science*, *16*(4), 863–874. https://doi.org/10.5194/os-16-863-2020

Moat, B. I., Smeed, D. A., Rayner, D., Johns, W. E., Smith, R., Volkov, D., et al. (2026). Atlantic meridional overturning circulation observed by the RAPID-MOCHA-WBTS (RAPID-meridional overturning circulation and heatflux array-western boundary time series) array at 26N from 2004 to 2024 (v2024.1a) [Dataset]. *British Oceanographic Data Centre - Natural Environment Research Council, UK*. https://doi.org/10.5285/48d0bf43-0598-ceb2-e063-7086abc062f1

Rayner, D., & Kanzow, T. (2011). The design strategy and methodology of the RAPID-MOC project moorings. *International Journal of the Society for Underwater Technology*, *29*(4), 159–171. https://doi.org/10.3723/ut.29.159

Reagan, J. R., Boyer, T. P., García, H. E., Locarnini, R. A., Baranova, O. K., Bouchard, C., et al. (2024). World ocean atlas 2023 [Dataset]. *NOAA National Centers for Environmental Information. NCEI Accession 0270533*. Retrieved from https://www.ncei.noaa.gov/products/world-ocean-atlas

Send, U., Kanzow, T., Zenk, W., & Rhein, M. (2002). Monitoring the Atlantic meridional overturning circulation at 16N. *CLIVAR Exchanges*, *7*(3/4), 31–33. Retrieved from https://oceanrep.geomar.de/id/eprint/5877/1/Exchanges25.pdf

Smeed, D. (2026). Code used in: Smeed et al 2026 Overturning circulation of the North Atlantic subtropical gyre computed in density coordinates at 26°N (Version v1) [Software]. *Zenodo*. https://doi.org/10.5281/zenodo.18432154

Tooth, O. J., Foukal, N. P., Johns, W. E., Johnson, H. L., & Wilson, C. (2024). Lagrangian decomposition of the Atlantic Ocean heat transport at 26.5°N. *Geophysical Research Letters*, *51*(14), e2023GL107399. https://doi.org/10.1029/2023gl107399

Van Sebille, E., Baringer, M. O., Johns, W. E., Meinen, C. S., Beal, L. M., Jong, M. F., & Aken, H. M. (2011). Propagation pathways of classical Labrador Sea water from its source region to 26°N. *Journal of Geophysical Research*, *116*(C12), C12027. https://doi.org/10.1029/2011jc007171

Volkov, D. L., Smith, R. H., Garcia, R. F., Smeed, D. A., Moat, B. I., Johns, W. E., & Baringer, M. O. (2024). Florida current transport observations reveal four decades of steady state. *Nature Communications*, *15*(1), 7780. https://doi.org/10.1038/s41467-024-51879-5

Xu, X., Rhines, P. B., & Chassignet, E. P. (2018). On mapping the diapycnal water mass transformation of the upper North Atlantic Ocean. *Journal of Physical Oceangraphy*, *48*(10), 2233–2258. https://doi.org/10.1175/jpo-d-17-0223.1

Zhang, R. (2010). Latitudinal dependence of Atlantic meridional overturning circulation (AMOC) variations. *Geophysical Research Letters*, *37*(16), L16703. https://doi.org/10.1029/2010gl044474

19448007, 2026, 5, Downloaded from https://agupubs.onlinelibrary.wiley.com/doi/10.1029/2025GL118277 by NICE, National Institute for Health and Care Excellence, Wiley Online Library on [11/03/2026]. See the Terms and Conditions (https://onlinelibrary.wiley.com/terms-and-conditions) on Wiley Online Library for rules of use; OA articles are governed by the applicable Creative Commons License